

**Iron and black carbon
in aerosol light
absorption**

Y. Derimian et al.

The role of iron and black carbon in aerosol light absorption

**Y. Derimian^{1,4}, A. Karnieli¹, Y. J. Kaufman², M. O. Andreae³, T. W. Andreae³,
O. Dubovik⁴, W. Maenhaut⁵, and I. Koren⁶**

¹Major part of this study was done while worked at: Jacob Blaustein Institute for Desert Research, Ben Gurion University of the Negev, Israel

²NASA Goddard Space Flight Center, NASA Goddard SFC, USA

³Max Planck Institute for Chemistry, Mainz, Germany

⁴Laboratoire de Optique Atmosphérique, Université de Lille 1/CNRS, Villeneuve d'Ascq, France

⁵Ghent University (UGent), Department of Analytical Chemistry, Institute for Nuclear Sciences, Gent, Belgium

⁶Department of Environmental Sciences, Weizmann Institute, Rehovot 76100, Israel

Received: 8 May 2007 – Accepted: 23 May 2007 – Published: 13 June 2007

Correspondence to: Y. Derimian (derimian@loa.univ-lille1.fr)

Title Page

Abstract

Introduction

Conclusions

References

Tables

Figures

◀

▶

◀

▶

Back

Close

Full Screen / Esc

Printer-friendly Version

Interactive Discussion

Abstract

Iron is a major component of atmospheric aerosols, influencing the light absorption ability of mineral dust, and an important micronutrient that affects oceanic biogeochemistry. The regional distribution of the iron concentration in dust is important for climate studies; however, this is difficult to obtain since it requires in-situ aerosol sampling or simulation of complex natural processes. Simultaneous studies of aerosol chemical composition and radiometric measurements of aerosol optical properties, which were performed in the Negev desert of Israel continuously for about eight years, suggest a potential for deriving a relationship between chemical composition and light absorption properties, in particular the spectral single-scattering albedo.

The two main data sets of the present study were obtained by a sun/sky radiometer and a stacked filter unit sampler that collects particles in coarse and fine size fractions. Analysis of chemical and optical data showed the presence of mixed dust and pollution aerosol in the study area, although their sources appear to be different. Spectral SSA showed an evident response to increased concentrations of iron, black carbon equivalent matter, and their mixing state. An empirical relationship that relates the spectral SSA, the percentage of iron in total particulate mass, and the pollution components was derived. Results calculated using this relationship were compared with measurements from dust episodes in several locations around the globe. The comparison reveals that dust over the eastern Mediterranean and Saudi Arabia contains less iron than that over Asia and the Sahara desert.

1 Introduction

The presence of iron (Fe) in aeolian dust is of wide interest in climate studies due to its biogeochemical and radiative impacts (Jickells et al., 2005; Mahowald et al., 2005). Iron oxide (primarily hematite) is a major component that affects the ability of aeolian dust to absorb sunlight at short wavelengths (the blue spectral region). Variable concentrations

Iron and black carbon in aerosol light absorption

Y. Derimian et al.

Title Page

Abstract

Introduction

Conclusions

References

Tables

Figures

⏪

⏩

◀

▶

Back

Close

Full Screen / Esc

Printer-friendly Version

Interactive Discussion

**Iron and black carbon
in aerosol light
absorption**Y. Derimian et al.

of iron oxide alter the dust's radiative properties (make dust darker or brighter) and thus may influence climate (Sokolik and Toon, 1999). Bio-available iron is an important micronutrient that affects oceanic biogeochemistry (Fan et al., 2006). Following dust deposition in oceanic regions (Fung et al., 2000; Colarco et al., 2003; Gao et al., 2003; Johnson et al., 2003; Kaufman et al., 2005b), iron fertilization supports phytoplankton growth and the cycles of other oceanic nutrients and bacteria (Martin and Gordon, 1988; Behrenfeld et al., 1996; Coale et al., 1996; Capone et al., 1997; Falkowski, 1997; Boyd et al., 2000; Jickells et al., 2005; Mongin et al., 2006). Subsequently, changes in the photosynthetic activity of phytoplankton alter the cycle of atmospheric CO₂ and of global carbon (Broecker and Henderson, 1998; Watson et al., 2000). The variability of iron concentrations supplied by aeolian dust may also be of importance for oceanic biota in various ocean regions where dust deposition is significant (Gao et al., 2001; Wiggert et al., 2006).

Transported aeolian dust can be contaminated by anthropogenic aerosols and thus contain products of industrial and motor vehicle combustion emissions, or products of biomass burning. Such aerosols contain light-absorbing carbon that is a strong absorber and therefore contributes to global warming (Jacobson, 2004; Chung and Seinfeld, 2005). Dubovik et al. (2002a) showed that the spectral absorption of pollution aerosols is distinctive from that of mineral dust. The spectral absorption properties of light-absorbing carbon depend on the origin of the material and combustion conditions (Andreae and Gelencser, 2006; Schkolnik et al., 2007). Strongly absorbing black soot particles are commonly called black carbon (BC) and are characterized by an increase of absorption towards long wavelengths proportional to $1/\lambda$ (Kirchstetter et al., 2004). In addition, the combustion of organic matter, such as biomass, or smoldering combustion may produce particles containing light-absorbing organic compounds. These particles have relatively strong absorption in the UV, and are denoted as brown carbon; they are suggested to be of higher relevance for regions outside of those that are highly industrialized and for cases where light absorption is not dominated by pure soot (Andreae and Gelencser, 2006). Here we will use the quantity “equivalent black carbon”

[Title Page](#)[Abstract](#)[Introduction](#)[Conclusions](#)[References](#)[Tables](#)[Figures](#)[◀](#)[▶](#)[◀](#)[▶](#)[Back](#)[Close](#)[Full Screen / Esc](#)[Printer-friendly Version](#)[Interactive Discussion](#)

(BC_e), operationally defined as the amount of strongly light-absorbing carbon with the approximate optical properties of soot carbon, which would give the same signal in our optical instrument as the sample.

Several approaches can be used for evaluation of iron or BC concentrations in particulate matter, e.g., in-situ sampling of atmospheric aerosol particles with further laboratory analysis. However, in-situ sampling requires considerable effort, and can even be impossible for providing results of wide spatial and temporal coverage. Another possibility is to employ chemistry transport model simulations. However, while models may better account for human induced factors and adequately estimate BC concentrations, prediction of natural iron concentrations depends on wind speeds and local mineralogy, and thus may carry more uncertainty (Kaufman et al., 2005a). An additional approach is modeling of aerosol optical properties (Sokolik and Toon, 1999), which can be employed for inversion of measurable aerosol optical characteristics and deriving concentrations of chemical elements. Modeling of complex refractive index, aerosol scattering and absorption coefficients for various combinations of minerals was recently improved by incorporation of the results of specifically designed measurements (Lafon et al., 2006). In their study Lafon et al. (2006) composed dust mixtures from some key minerals, including hematite and goethite, typically found in soils and aerosol samples. Laboratory-obtained information on the fraction of minerals in different size modes was included in the modeling of aerosol optical properties. Schuster et al. (2005) demonstrated an approach of inversion of AERONET retrievals into chemical elements concentrations (namely BC) and specific absorption, using an effective medium approximation. This approximation enables effective optical constants calculation of internally mixed chemical elements in various volume fractions. An advantage of the approach suggested by Schuster et al. (2005) lies in tying the effective medium approximation to real optical measurements of ambient aerosols.

Other studies showed the possibility of deconvoluting dust and BC spectral absorption and scattering properties, and thereby inferring iron and BC concentrations. For instance, Fialho et al. (2005) differentiated the absorption spectral dependence of dust

Iron and black carbon in aerosol light absorption

Y. Derimian et al.

Title Page

Abstract

Introduction

Conclusions

References

Tables

Figures

◀

▶

◀

▶

Back

Close

Full Screen / Esc

Printer-friendly Version

Interactive Discussion

and BC measured by an aethalometer. In a subsequent study, Fialho et al. (2006) calibrated these measurements with Fe on the filters, and derived empirical calibration constants for the determination of the iron concentration from the aethalometer observations. Koven and Fung (2006) employed a similar concept of absorption spectral dependence for the characterization of dust composition; however, they studied sun/sky radiometer measurements through the whole atmospheric column (AERONET) and incorporated the mineralogical effects by using different modeled relative fractions of hematite, silicate and BC.

The approach used in the present paper is similar to that of Koven and Fung (2006) and Schuster et al. (2005) in referring to aerosol scattering and absorption spectral properties derived from a sun/sky radiometer. However, we do not employ the effective medium approximation to connect the optical measurements to the aerosol chemical composition, but use the chemical element concentrations measured on filter samples of atmospheric aerosols. Specifically, we take advantage of a large data set of co-located and simultaneous long-term AERONET observations and aerosol sampling results. We use these data for deriving an empirical relationship between spectral single scattering albedo and concentrations of Fe and BC_e . This approach avoids usage of bulk or modeled optical properties of a material, or absorption properties measured on aerosol samples after they have been removed from atmosphere. Instead, we utilize in-situ aerosol optical characteristics that correctly reflect the actual measured radiation field. We also do not reconstruct aerosol mineralogy or use soil characteristics, but refer to actual Fe and BC_e concentrations in real atmospheric aerosols.

The general motivation for this paper was to assess iron concentrations in atmospheric dust by aerosol spectral absorption. The iron concentration in total dust mass can be useful for estimating the amounts of iron deposited to the ocean. We have analyzed the differential aerosol spectral absorption from the blue to the NIR (near infrared) spectral region, which should be proportional to the associated concentrations of iron and BC_e . In this study, we consider concentrations of total iron, and assume that the optically relevant iron oxides represent a fixed part of the total iron in airborne

**Iron and black carbon
in aerosol light
absorption**Y. Derimian et al.

[Title Page](#)[Abstract](#)[Introduction](#)[Conclusions](#)[References](#)[Tables](#)[Figures](#)[◀](#)[▶](#)[◀](#)[▶](#)[Back](#)[Close](#)[Full Screen / Esc](#)[Printer-friendly Version](#)[Interactive Discussion](#)

mineral dust. This iron oxide to total iron ratio may be unique for a given location with its specific sources, but at the end of Sect. 4.6 we discuss the reliability and restrictions of this assumption. The aerosol spectral absorption was obtained by inversion of sun/sky photometer measurements (AERONET product). The aerosol chemical composition was obtained from aerosol sampling at ground level. Specific objectives were: (1) to correlate data sets for events where ground level aerosol chemistry was found to be representative for the total column optical measurement; (2) to estimate the contamination of atmospheric dust by BC and its role in aerosol spectral absorption; and (3) to derive an empirical relationship between iron concentrations and differential aerosol spectral absorption.

2 Site location

Measurements were conducted at the Sede Boker (in some sources referred to as Sde Boker) Campus of the Ben-Gurion University of the Negev (30°51' N, 34°47' E, 470 m a.m.s.l.), Israel. The site is located in the eastern Mediterranean region, characterized by relatively high levels of tropospheric aerosol burden due to the influence of anthropogenic aerosols that originate mainly from Europe, and mineral dust from the North African, Sinai, and Saudi Arabian deserts (Ichoku et al., 1999; Formenti et al., 2001; Andreae et al., 2002; Gerasopoulos et al., 2003; Israelevich et al., 2003; Kubilay et al., 2003). Specifically, Sede Boker is situated in the northern part of the Negev Desert, relatively far from highly populated and industrial areas. The climate is dry, with a mean annual precipitation of 100–200 mm and 20–40 rainy days throughout the year. The average relative humidity at 14:00 local time for July is 30–35% and for January, 40–50% (Stern et al., 1986).

Iron and black carbon in aerosol light absorption

Y. Derimian et al.

Title Page

Abstract

Introduction

Conclusions

References

Tables

Figures

◀

▶

◀

▶

Back

Close

Full Screen / Esc

Printer-friendly Version

Interactive Discussion

3 Data sets and instrumentation

The main data sets were obtained from a CIMEL sun/sky photometer, part of the global Aerosol Robotic Network (AERONET), and a “Gent” PM10 stacked filter unit (SFU) sampler. Additional data were obtained from a single-wavelength integrating nephelometer and a scanning electron microscope (SEM) equipped with an energy dispersive spectrometer (EDS).

3.1 Sun/sky photometer

The AERONET program is an automatic robotic sun and sky scanning measurement initiative (Holben et al., 1998). A CIMEL spectral photometer performs direct sun measurements every 15 min, with a 1.2° field of view at 340, 380, 440, 500, 675, 870, 940, and 1020 nm nominal wavelengths. The spectral aerosol optical thickness (AOT or τ_{ext}) was retrieved at seven of these wavelengths from the direct sun measurements; the 940 nm channel was used to retrieve water vapor content. The angular distribution of sky radiance was also measured at 440, 670, 870, and 1020 nm. The measured spectral sun and sky radiances were used to retrieve aerosol optical parameters at four wavelengths by the AERONET inversion code (Dubovik and King, 2000).

In this paper we utilize data from Version 2 (V2) inversion products. V2 inversion partitions aerosol particles into spherical and non-spherical components, which are modeled by an ensemble of polydisperse, homogeneous spheres and a mixture of polydisperse, randomly-oriented homogeneous spheroids (Mishchenko et al., 1997) with a fixed spheroid aspect ratio distribution (Dubovik et al., 2006). The retrievals utilized also contain redefined surface reflectance properties, which are obtained by the inclusion of combined satellite data, and which account for possible improvements in retrieved aerosol properties and single-scattering albedo in particular (Sinyuk et al., 2007). In addition, all restrictions recommended in Dubovik et al. (2002a) for reliability of the inversion product were applied. More details on the development of the retrieval algorithm, modifications and accuracy assessments can be found in Dubovik and King

Iron and black carbon in aerosol light absorption

Y. Derimian et al.

Title Page

Abstract

Introduction

Conclusions

References

Tables

Figures

◀

▶

◀

▶

Back

Close

Full Screen / Esc

Printer-friendly Version

Interactive Discussion

(2000), Smirnov et al. (2000), Dubovik et al. (2000, 2002a, 2002b), and Sinuyk et al. (2007).

3.2 “Gent” PM10 stacked filter unit sampler

The “Gent” PM10 stacked filter unit (SFU) sampler collects particles on Nuclepore polycarbonate filters in a coarse (2–10 μm aerodynamic diameter (AD)) and a fine (<2 μm AD) size fraction. The SFU sampler is operated continuously on a two-two-three-day scheme. The instrument was located at about 8 m above the ground and operated at an air flow rate of $\sim 16 \text{ L min}^{-1}$. To avoid the problem of filter clogging and consequently non-representative measurements in the two-two-three-day scheme, the sampling was always conducted with a timer set at 50% for the two-day sample and at 33% for the three-day sample, thus the SFU effectively sampled only 50 or 33% of the time evenly distributed over two or three days, respectively. This generally results in little clogging or effects from a decrease in flow rate during the sampling, except possibly during episodes of extremely high aerosol concentrations. The volume of the sampled air is obtained from a volume meter, which is accurate within 5% and is not affected by the concentration of the aerosol in the air or by the filter loading. The SFU samples were analyzed for particulate mass (PM), in $\mu\text{g m}^{-3}$, for over 40 elements including Fe, in ng m^{-3} , and black carbon equivalent (BC_e), also in $\mu\text{g m}^{-3}$. The PM was measured using gravimetry at 20°C and 50% relative humidity. The uncertainty associated with the weighing is usually less than 3% for the coarse PM and less than 5% for the fine PM. More than 40 elements were measured using a combination of instrumental neutron activation analysis (INAA) and particle-induced X-ray emission analysis (PIXE). BC_e , that is black carbon corresponding to a measured light extinction at fixed absorption efficiency, was measured by a light reflectance technique. The measurements were performed with a commercial smoke stain reflectometer (Diffusion Systems Ltd, London, UK, model 43) that uses white light. Instead of assuming a mass absorption efficiency (MAE, in $\text{m}^2 \text{g}^{-1}$), the instrument was calibrated with secondary standards for BC_e determination. These secondary standards were produced by depositing soot

Iron and black carbon in aerosol light absorption

Y. Derimian et al.

Title Page

Abstract

Introduction

Conclusions

References

Tables

Figures

◀

▶

◀

▶

Back

Close

Full Screen / Esc

Printer-friendly Version

Interactive Discussion

from acetylene burning on filters. More details about the SFU samples and the chemical analysis, including studies conducted at the Sede Boker site, have been discussed by Maenhaut et al. (1996a, b, 1997) and Andreae et al. (2002).

3.3 Nephelometer

5 The Integrating Nephelometer (M903, Radiance Research, Seattle, WA, USA) measures the light scattering extinction coefficient (σ_{scat}) with a 2-min resolution at a wavelength of 545 nm, with a scattering angular range of 7–170°. The instrument is operated indoors and air is supplied through a plastic tubing of up to 3 m length and of 2.2 cm internal diameter. The inlet of the tubing is located outdoors at about 10 m above ground
10 level and faces downwards. Pressure, temperature, and relative humidity (RH) in the scattering volume of the instrument are also monitored and recorded. In order to eliminate a non-linear increase in σ_{scat} due to high humidity, the data with RH > 80% were removed (Andreae et al., 2002).

3.4 Scanning electron microscope

15 The high-resolution field emission scanning electron microscope (SEM) LOE 1530, equipped with an energy dispersive X-ray (EDX) spectrometer, at the Max Planck Institute for Chemistry, Mainz, was used for visualization and qualitative analysis of individual aerosol particles collected on the Nuclepore polycarbonate filters of the SFU samples. The working conditions for the images presented here were set at an accelerating voltage of 5 or 15 kV and magnification varied from about 70 000X to 400 000X.
20 This enabled the observation of particles and their structures in sizes from a few tens to hundreds of nanometers.

Iron and black carbon in aerosol light absorption

Y. Derimian et al.

Title Page

Abstract

Introduction

Conclusions

References

Tables

Figures

◀

▶

◀

▶

Back

Close

Full Screen / Esc

Printer-friendly Version

Interactive Discussion

4 Data analysis and discussion

This section presents an analysis of aerosol absorption obtained from radiometric measurements (Sect. 4.1.), aerosol chemistry obtained from in-situ surface sampling (Sects. 4.2. and 4.3.), their integration (Sect. 4.4.), and the derivation of an empirical relationship between aerosol spectral absorption and chemistry (Sect. 4.5). The proposed relationship is examined with data from several episodes and locations (Sect. 4.6).

4.1 Radiometric observations

The single-scattering albedo (SSA or ω_0) is the ratio of light scattering to total light extinction (scattering and absorption) and represents scattering effectiveness relative to total extinction. Therefore, SSA decreases when absorption increases. Mineral dust and aerosol particles originating from combustion processes have different wavelength dependencies for SSA (Dubovik et al., 2002a). This difference in aerosol spectral absorption is predominantly related to absorption by two components, iron oxide and black carbon. The SSA for mineral dust usually decreases towards short wavelengths due to the presence of iron oxide. The SSA for anthropogenic pollution aerosols that contain BC decreases towards long wavelengths. Thus, the presence of iron oxide or BC in aerosols can be determined by examining the behavior of the spectral SSA.

The mean spectral single-scattering albedo obtained during about eight years of measurements at Sede Boker for periods with predominantly coarse (Ångström exponent (\AA) <0.6) and fine (\AA) >1.0) aerosol, respectively, is presented in Fig. 1. The Ångström exponent represents the wavelength dependence of extinction and is calculated by

$$\text{\AA} = - \frac{\ln \frac{\tau_{\text{ext}}^{870}}{\tau_{\text{ext}}^{440}}}{\ln \frac{\lambda^{870}}{\lambda^{440}}} \quad (1)$$

Iron and black carbon in aerosol light absorption

Y. Derimian et al.

Title Page

Abstract

Introduction

Conclusions

References

Tables

Figures

◀

▶

◀

▶

Back

Close

Full Screen / Esc

Printer-friendly Version

Interactive Discussion

In our study we employ the difference between SSA at 440 nm and 1020 nm (dSSA), which provides two advantages: first, it is expected that the difference will provide better accuracy than absolute values, since retrieval of spectral dependence is more reliable than that of an absolute value; and second, the spectral behavior of an SSA curve can be characterized by only one parameter, dSSA. Negative values of the difference SSA(440 nm)–SSA(1020 nm) will be related to stronger absorption by iron oxide at 440 nm, while positive values are related to stronger absorption by BC-containing particles at 1020 nm.

Figure 2 shows all quality-assured observations of SSA(440 nm)–SSA(1020 nm) versus the Ångström exponent, which were made at the Sede Boker site from October 1995 to May 2006. The data presented in this figure are stratified into different ranges of SSA(1020 nm) in order to indicate events with different levels of absorption at 1020 nm. This figure reveals that, as the Ångström exponent (870 nm–440 nm) increases from about zero to about 1.5 (indicating a decreasing contribution of coarse dust particles and increasing fraction of fine pollution particles), spectral SSA gradually changes from stronger absorption at 440 nm to stronger absorption at 1020 nm. It is noteworthy that absorption at 1020 nm is quite weak (marked by red diamonds and blue circles) for events dominated by coarse particles (Ångström exponent about zero). As the contribution from fine particles increases (Ångström exponent from 0.5 to 1.0), absorption is still strongest at 440 nm, but absorption at 1020 nm becomes significant (part of observations marked by green squares). This spectral SSA behavior is related to mixtures of dust and pollution, with characteristic Ångström exponent values in the range from 0.5 to 1.0. As the Ångström exponent continues to increase, which means that the contribution of fine particles increases, absorption at 1020 nm becomes stronger than at 440 nm and SSA(1020 nm) may reach values of 0.85 (black triangles). Consequently, Fig. 2 classifies spectral SSA for events having dust- or pollution-dominated contributions and different degrees of mixing.

**Iron and black carbon
in aerosol light
absorption**Y. Derimian et al.

[Title Page](#)[Abstract](#)[Introduction](#)[Conclusions](#)[References](#)[Tables](#)[Figures](#)[◀](#)[▶](#)[◀](#)[▶](#)[Back](#)[Close](#)[Full Screen / Esc](#)[Printer-friendly Version](#)[Interactive Discussion](#)

4.2 In-situ surface sampling

Concentrations of BC_e and total Fe at ground level were measured simultaneously with the radiometric measurements. Figure 3 shows the percentage of BC_e versus the percentage of Fe in the PM10 total particulate mass (TPM). The BC_e or Fe percentages in the TPM (denoted hereafter as %TPM) were calculated as the sum of BC_e or Fe concentrations ($\mu\text{g m}^{-3}$) in the fine and coarse size fractions relative to the sum of the particulate mass concentrations ($\mu\text{g m}^{-3}$) in the two size fractions. This figure shows a pattern of negative correlation between the percentages of BC_e and Fe in the TPM. This implies that, generally, sources of BC_e (pollution tracer) and Fe (mainly from dust) are different. Another conclusion, suggested by this plot, is that during most of the events both elements are present at measurable concentrations, i.e., that we generally have a mixture of dust and pollution aerosol at our sampling site.

It should be mentioned here that the BC_e concentration is measured by a light reflectance technique so that other species (e.g., Fe) or even just an increase of total mass concentration ($\mu\text{g m}^{-3}$) on the filter during a dust event may contribute to the BC_e signal by additional light absorption. To test for these potential interferences, we examine the possible influence of Fe and high mass concentrations on the BC_e signal (Fig. 4). This figure shows BC_e , %TPM in the fine fraction, versus Fe, %TPM in the coarse fraction. Different ranges of total mass concentration are indicated by different symbols. Figure 4 reveals that (1) fine BC_e of pollution origin is not positively correlated with dust-related coarse Fe; (2) increase in mass concentration does not coincide with an increase of BC_e , %TPM in fine fraction; and (3) increase in total mass concentration is clearly coincident with an increase in coarse Fe, %TPM. Later, in Fig. 7, we will also show that the main part of BC_e is found in the fine and that of Fe in the coarse size fraction. Thus, an increase in Fe, %TPM or total mass concentration does not cause a spurious increase in the measured BC_e , %TPM.

Iron and black carbon in aerosol light absorption

Y. Derimian et al.

Title Page

Abstract

Introduction

Conclusions

References

Tables

Figures

◀

▶

◀

▶

Back

Close

Full Screen / Esc

Printer-friendly Version

Interactive Discussion

4.3 Individual particle analysis

Four pairs of SFU sample filters (coarse and fine) from four dust storm events were analyzed by scanning electron microscope (SEM) in order to examine microphysical characteristics and possible mixing of the sampled aerosols. In this paper we present a few images from analyzed dust events on 2 April 2000 and 3 February 2001 in order to illustrate dust and pollution mixing and examples of the observed soot particles. Figure 5 shows images of individual particles collected on the fine and coarse filters. It demonstrates the presence of typical ring and open soot clusters that were found among dust particles on the coarse filter from the dust event on 2 April 2000, and soot clusters attached to dust that were found on the fine filter from the dust event on 3 February 2001. Quite similar pictures were observed on other analyzed filters, where soot clusters were observed between mineral dust particles, as well as attached to dust particles.

4.4 Data integration

A combined data set was created for the purpose of deriving empirical relationships between aerosol spectral absorption and chemical composition. A challenge in the creation of an adequate data set was the adjustment between optical measurements made through the total atmospheric column and aerosol sampling at ground level. Representativeness of surface sampling for dust events is problematic due to the fact that dust maybe transported at high altitudes (Hamonou et al., 1999; di Sarra et al., 2001; Tsidulko et al., 2002; Dulac and Chazette, 2003; Alpert et al., 2004) and not be adequately sampled at the surface. An additional problem is that the aerosol-sampling unit collects particles during two or three days on one filter, thus it may contain particles from different events and sources. In order to avoid involving filters that contain particles from different events, a time series of AOT was analyzed for each preliminarily selected episode of elevated AOT. Data were selected only if the AOT time series indicated one dust or pollution episode during the two or three day period of sampling.

Iron and black carbon in aerosol light absorption

Y. Derimian et al.

Title Page

Abstract

Introduction

Conclusions

References

Tables

Figures

◀

▶

◀

▶

Back

Close

Full Screen / Esc

Printer-friendly Version

Interactive Discussion

**Iron and black carbon
in aerosol light
absorption**Y. Derimian et al.

An additional analysis was conducted to assure representative surface sampling of dust events ($\text{\AA} < 0.6$). This analysis employs the ratio of $\tau_{\text{ext}}/\sigma_{\text{scatt}0}$ as a function of time, where τ_{ext} is aerosol optical thickness measured through the entire atmospheric column and $\sigma_{\text{scatt}0}$ is the aerosol scattering coefficient measured by the nephelometer at ground level. This ratio can be used for estimating the equivalent aerosol height, while its time series reflects vertical dynamics of aerosols passing over the site. For example, if the main aerosol concentration is near the surface or aloft, the value of the ratio will be low or high, and indicate an equivalent aerosol height. More detailed discussion and examples of the ratio $\tau_{\text{ext}}/\sigma_{\text{scatt}0}$ usage can be found in (Derimian et al., 2006). Thus, by parallel analysis of the ratio $\tau_{\text{ext}}/\sigma_{\text{scatt}0}$ and τ_{ext} as a function of the time, we are able to follow the dynamics of dust events and to distinguish between high altitude dust transport and dust settling episodes. This tool enables the selection of representative filters where chemical characteristics of settled dust were expected to reflect the measured optical properties. Based on the knowledge that pollution aerosols in the study area are generally transported at lower heights (Formenti et al., 2001, 2002a, b) and surface sampling is representative for them, events with $\text{\AA} > 0.7$ were not subjected to additional analysis for vertical dynamics.

Figure 6 presents averaged values of the difference $\text{SSA}(440) - \text{SSA}(1020)$ versus the Ångström exponent (870–440) for 25 selected events that cover a wide range of optical data measured during elevated loadings of dust and pollution aerosols. This optical data set was matched with aerosol chemistry and selected from the general data set (Figs. 2 and 3) by the above-mentioned criteria. Representation of the covered concentration range of the chemical elements BC_e and Fe is shown in Fig. 3. The selected data are marked using red circles ($\text{\AA} > 0.7$ – fine particles dominating) and squares ($\text{\AA} < 0.6$ – coarse particles dominating), over the background of all observations. Unfortunately, optical data for extremely high BC_e concentrations were not available, probably due to some systematic problem such as meteorological conditions, or sky homogeneity that prevented sun/sky photometer measurements, or that violated the criterion for proper almucantar retrievals. However, the existing optical data were

[Title Page](#)[Abstract](#)[Introduction](#)[Conclusions](#)[References](#)[Tables](#)[Figures](#)[◀](#)[▶](#)[◀](#)[▶](#)[Back](#)[Close](#)[Full Screen / Esc](#)[Printer-friendly Version](#)[Interactive Discussion](#)

matched to a range of points in Fig. 3 with the highest density of data, i.e., the range of most frequent concentrations. Thus, at this stage we have a set of carefully matched optical and chemical data for 25 dust and pollution loaded events.

Figure 7 presents the BC_e and Fe percentages in the fine and coarse size fractions and the corresponding differences: $SSA(440) - SSA(1020)$, $SSA(440) - SSA(670)$, and $SSA(670) - SSA(1020)$. Data on this plot were sorted by decreasing total (fine and coarse) iron concentration. A trend from negative to positive values of $SSA(440) - SSA(1020)$ can be noticed as the total concentration of iron decreases and the role of the BC_e contribution increases. In addition, spectral SSA subdivided by two ranges, one from 440 nm to 670 nm and the second from 670 nm to 1020 nm, reveals the response to relative contributions of iron and BC_e . The difference $SSA(440) - SSA(670)$ shows negative values in response to dominant iron contribution and gradually becomes positive as the role of BC_e increases. The $SSA(670) - SSA(1020)$ response is similar to $SSA(440) - SSA(670)$ and $SSA(440) - SSA(1020)$ only when the contribution of BC_e is high, however it varies little and is close to zero when the iron contribution is dominant. This implies that spectral SSA from 440 nm to 670 nm responded to both iron and BC_e , while spectral SSA from 670 nm to 1020 nm generally responded to BC_e . Figure 7 also shows that the major concentration of iron is in the coarse size fraction, which supports its mineral dust origin, while most of BC_e is in the fine fraction, which is typical for anthropogenic pollution. In summary, Fig. 7 reveals that SSA retrievals from AERONET are consistent with aerosol chemical composition and suggests a potential for deriving a relationship between retrieved SSA, Fe, and BC_e .

4.5 Empirical relationship analysis

The matched data set was employed to derive an empirical relationship between the spectral SSA, and the Fe and BC_e percentage in the total particulate mass. The original goal was the assessment of the Fe percentage in atmospheric dust by spectral absorption; however, because the dust was found to be contaminated by pollution, BC_e had to be included in the analysis.

Iron and black carbon in aerosol light absorption

Y. Derimian et al.

Title Page

Abstract

Introduction

Conclusions

References

Tables

Figures

◀

▶

◀

▶

Back

Close

Full Screen / Esc

Printer-friendly Version

Interactive Discussion

The analysis includes spectral absorption, represented by the difference SSA(440) – SSA(1020), and the concentrations of Fe and BC_e using the following model:

$$\text{SSA}(440) - \text{SSA}(1020) = a_1 * \text{Fe}\% + a_2 * \text{BC}_e\% + a_3, \quad (2)$$

where a₁, a₂, and a₃ are regression coefficients. Multivariate regression analysis yields a₁ = -0.0635±0.0116, a₂ = -0.0020±0.0065, and a₃ = 0.1352±0.0429 (± Standard Error); the regression is significant at p<0.0001, the coefficient of multiple determination (r²) is 0.73. It means that Fe and BC_e in this model explain 73% of the variance in SSA(440)–SSA(1020). The rest of the variance may be due to facts such as (1) Fe is not directly related to the optically relevant iron oxide (Lafon et al., 2004), (2) other components of mineral dust may contribute to dust absorption (Jacobson, 2001), (3) spectral absorption of pollution cannot be completely explained by measured BC_e, (Bond, 2001; Kirchstetter et al., 2004), and (4) measurement uncertainties. Nevertheless, 73% of explained variance is quite a strong response of spectral SSA to aerosol chemistry. A drawback of the above model is that this approach requires information on BC_e in order to derive the Fe concentration. The regression model gives a higher Fe percentage without the inclusion of BC_e due to its extra absorption. However, it should be noted that the weight of BC_e (coefficient a₂) is small in this model and any error in the BC_e estimate has only a minor impact.

4.6 Evaluation of the empirical relationship

In order to evaluate our attempt to assess the Fe concentration, we utilized appropriate and available spectral SSAs that were retrieved from ground-based and satellite optical measurements for several episodes and locations (Table 1). Specifically, we used data from Sede Boker (Negev desert) (an average for about eight years), Solar Village (Saudi Arabia) (Sinyuk et al., 2007), Korean Strait (Asia) during ACE-Asia (Bergstrom et al., 2004), and the Sahara desert (Senegal) (Kaufman et al., 2001). An accumulated error was also estimated in order to assess the uncertainty in calculated Fe percentage. This error is caused by uncertainty in the variables (SSA difference and BC_e)

Iron and black carbon in aerosol light absorption

Y. Derimian et al.

Title Page

Abstract

Introduction

Conclusions

References

Tables

Figures

◀

▶

◀

▶

Back

Close

Full Screen / Esc

Printer-friendly Version

Interactive Discussion

and uncertainty in the assumed linear dependence between SSA difference, Fe and BC_e (i.e., errors of the regression coefficients a_1 , a_2 , and a_3). Since BC_e measured concentrations were not available, they were assumed to be $2 \pm 2\%$. The error of the SSA difference was assumed as ± 0.03 , which is the error of the SSA values (Dubovik et al., 2002a). However, we used the SSA difference to describe the retrieved spectral dependence, and we expect that its accuracy will actually be better than either of the absolute SSA values.

The calculated percentages of Fe for several episodes and locations are presented in Table 1 for the assumed BC_e concentration, and accompanied by the standard errors representing a worst-case scenario. These errors were in the range of $\pm 28\%$ to 36% . For others scenarios of typical dust events the errors were lower and, on average, $\pm 25\%$ to 30% ; however, they may increase for low Fe concentrations and events where BC spectral absorption is dominating. In Table 1 the calculated percentages of Fe are compared with values reported in the literature. For example, Ganor and Foner (1996) gave a median Fe content of 2.9% for dust storms in Israel. This value is a result of completely independent measurements, and agrees well with the value calculated by our empirical relationship. The calculated Fe percentage for the Korean Strait area during ACE-Asia, 12 April 2001 is comparable to the estimated Fe in eastern Asia during ACE-Asia in spring 2001 (Zhang et al., 2003), where the reported concentrations were from 3.9 ± 0.5 to $4.0 \pm 0.9\%$. The calculated Fe percentage for Sahara dust is comparable to the reported value of $4.45 \pm 0.49\%$ (Guieu et al., 2002), which was proposed as characterizing Saharan dust. It is, however, lower than the values reported by (Lafon et al., 2004), who found a mean Fe of $6.3 \pm 0.9\%$ in Niger, where the probable source was the Chad basin, and $7.8 \pm 0.4\%$ in the Sahelian zone. In summary, the calculated percentages of Fe and those reported in the literature are comparable, and yield a similar trend of less iron content in the eastern Mediterranean and Saudi Arabia than in Asia and the Saharan deserts. Considering the good agreement of the calculated results to results reported in the literature, one also may expect improvement of modeling accuracy by our empirical relationship with increasing number and quality of

Iron and black carbon in aerosol light absorption

Y. Derimian et al.

[Title Page](#)[Abstract](#)[Introduction](#)[Conclusions](#)[References](#)[Tables](#)[Figures](#)[◀](#)[▶](#)[◀](#)[▶](#)[Back](#)[Close](#)[Full Screen / Esc](#)[Printer-friendly Version](#)[Interactive Discussion](#)

observations.

One additional aspect should be discussed here for the proper interpretation of the results obtained. That is, how representative is the total iron concentration for the iron oxide content of the aerosol? Iron oxide is present as a major aerosol component affecting the short-wavelength absorption of mineral dust. However, iron oxide represents only a part of the total iron, which may also exist in the crystal lattice of numerous other desert minerals. The iron oxide-to-total iron ratio in natural and soil-derived aerosols was characterized by (Lafon et al., 2004, 2006). They reported considerable variability of iron oxide-to-total iron ratio for various regions and sampling conditions. Lafon et al. (2006), however, conclude that there is no clear relationship between the oxide-to-total iron ratio and dust origin or aging; thus, probably both effects may play a role and additional studies are required. Based on all values of oxide-to-total iron ratio reported in (Lafon et al., 2004; 2006) we calculated an average of 0.54 (± 0.10) (\pm Std.Dev.), and with some outliers removed the variability can be reduced to around 10%. Thus, given the present lack of better knowledge, a fixed oxide-to-total iron ratio is a reasonable assumption for a specific region or observation, and the ratio given can be considered as an overall rough estimate with some degree of variability.

5 Summary and conclusions

The importance of the radiative and biogeochemical impact of iron on the climate system requires the estimation of the iron distribution, especially in regions of the globe that are strongly affected by mineral dust. The observed mixtures of dust and pollution aerosols over the Negev desert of Israel enabled the characterization of the relationship between spectral absorption and chemical composition. We have presented the response of remotely sensed aerosol spectral absorption to varying iron concentrations, and suggested an approach for the estimation of the iron content of the dust aerosol. The following is a summary of specific conclusions inferred in this study.

1. Mineral-dust-derived Fe (mostly in the coarse size fraction) and pollution-

Iron and black carbon in aerosol light absorption

Y. Derimian et al.

Title Page

Abstract

Introduction

Conclusions

References

Tables

Figures

◀

▶

◀

▶

Back

Close

Full Screen / Esc

Printer-friendly Version

Interactive Discussion

**Iron and black carbon
in aerosol light
absorption**

Y. Derimian et al.

[Title Page](#)[Abstract](#)[Introduction](#)[Conclusions](#)[References](#)[Tables](#)[Figures](#)[◀](#)[▶](#)[◀](#)[▶](#)[Back](#)[Close](#)[Full Screen / Esc](#)[Printer-friendly Version](#)[Interactive Discussion](#)

originated BC_e (mainly in the fine fraction) were found to be supplied to the Negev desert from different sources. Individual particle analysis of some dust events demonstrated the presence of typical ring and open soot clusters, both externally-mixed and attached to dust particles.

2. The difference $SSA(440\text{ nm})-SSA(1020\text{ nm})$, which indicates SSA spectral behavior, showed a trend from negative (stronger absorption in 440 nm) to positive (stronger absorption in 1020 nm) values as the total iron concentration decreased and the role of BC_e increased.
3. The Fe percentage in the total particulate mass, calculated using an empirical multivariate regression model, is comparable to values presented in the literature. The results suggest less iron content in dust from the eastern Mediterranean and Saudi Arabia than from Asia and the Sahara.

An advantage of the derived empirical relationship between spectral SSA, Fe, and BC_e is the use of actual ambient aerosol measurements, namely, the retrieved spectral absorption from the total column, and in-situ Fe and BC_e concentrations. Such an approach does not involve modeling of aerosol composition and optical characteristics. The approach suggested here may be employed for the estimation of the iron concentration in mineral dust, and further may enable quantification of the iron distribution and deposition during dust storm events.

Acknowledgements. The authors thank all members of the AERONET group, led by B. N. Holben, for data processing and operation of the AERONET site in Israel. The filter analysis was supported by the Belgian Federal Science Policy Office. Also, the authors are thankful to J. Huth from the Max Planck Institute for Chemistry, Mainz, Germany, for the SEM images.

References

Alpert, P., Kishcha, P., Shtivelman, A., Krichak, S. O., and Joseph, J. H.: Vertical distribution of Saharan dust based on 2.5-year model predictions, *Atmos. Res.*, 70, 2, 109–130, 2004.

- Andreae, M. O. and Gelencser, A.: Black carbon or brown carbon? The nature of light-absorbing carbonaceous aerosols, *Atmos. Chem. Phys.*, 6, 3131–3148, 2006, <http://www.atmos-chem-phys.net/6/3131/2006/>.
- Andreae, T. W., Andreae, M. O., Ichoku, C., Maenhaut, W., Cafmeyer, J., Karnieli, A., and Orlovsky, L.: Light scattering by dust and anthropogenic aerosol at a remote site in the Negev desert, Israel, *J. Geophys. Res.*, 107(D1–D2), 4008, doi:10.1029/2001JD900252, 2002.
- Behrenfeld, M. J., Bale, A. J., Kolber, Z. S., Aiken, J., and Falkowski, P. G.: Confirmation of iron limitation of phytoplankton photosynthesis in the equatorial Pacific Ocean, *Nature*, 383, 6600, 508–511, 1996.
- Bergstrom, R. W., Pilewskie, P., Pommier, J., Rabbette, M., Russell, P. B., Schmid, B., Redemann, J., Higurashi, A., Nakajima, T., and Quinn, P. K.: Spectral absorption of solar radiation by aerosols during ACE-Asia, *J. Geophys. Res.*, 109, D19S15, doi:10.1029/2003JD004467, 2004.
- Bond, T. C.: Spectral dependence of visible light absorption by carbonaceous particles emitted from coal combustion, *Geophys. Res. Lett.*, 28, 21, 4075–4078, 2001.
- Boyd, P. W., Watson, A. J., Law, C. S., Abraham, E. R., Trull, T., Murdoch, R., Bakker, D. C. E., Bowie, A. R., Buesseler, K. O., Chang, H., Charette, M., Croot, P., Downing, K., Frew, R., Gall, M., Hadfield, M., Hall, J., Harvey, M., Jameson, G., LaRoche, J., Liddicoat, M., Ling, R., Maldonado, M. T., McKay, R. M., Nodder, S., Pickmere, S., Pridmore, R., Rintoul, S., Safi, K., Sutton, P., Strzepek, R., Tanneberger, K., Turner, S., Waite, A., and Zeldis, J.: A mesoscale phytoplankton bloom in the polar Southern Ocean stimulated by iron fertilization, *Nature*, 407, 6805, 695–702, 2000.
- Broecker, W. S. and Henderson, G. M.: The sequence of events surrounding Termination II and their implications for the cause of glacial-interglacial CO₂ changes, *Paleoceanography*, 13, 4, 352–364, 1998.
- Capone, D. G., Zehr, J. P., Paerl, H. W., Bergman, B., and Carpenter, E. J.: Trichodesmium, a globally significant marine cyanobacterium, *Science*, 276, 5316, 1221–1229, 1997.
- Chung, S. H. and Seinfeld, J. H.: Climate response of direct radiative forcing of anthropogenic black carbon, *J. Geophys. Res.*, 110, D11102, doi:10.1029/2004JD005441, 2005.
- Coale, K. H., Johnson, K. S., Fitzwater, S. E., Gordon, R. M., Tanner, S., Chavez, F. P., Ferioli, L., Sakamoto, C., Rogers, P., Millero, F., Steinberg, P., Nightingale, P., Cooper, D., Cochlan, W. P., Landry, M. R., Constantinou, J., Rollwagen, G., Trasvina, A., and Kudela, R.: A massive phytoplankton bloom induced by an ecosystem-scale iron fertilization experiment in the

**Iron and black carbon
in aerosol light
absorption**Y. Derimian et al.

Title Page

Abstract

Introduction

Conclusions

References

Tables

Figures

◀

▶

◀

▶

Back

Close

Full Screen / Esc

Printer-friendly Version

Interactive Discussion

- equatorial Pacific Ocean, *Nature*, 383, 6600, 495–501, 1996.
- Colarco, P. R., Toon, O. B., Reid, J. S., Livingston, J. M., Russell, P. B., Redemann, J., Schmid, B., Maring, H. B., Savoie, D., Welton, E. J., Campbell, J. R., Holben, B. N., and Levy, R.: Saharan dust transport to the Caribbean during PRIDE: 2. Transport, vertical profiles, and deposition in simulations of in situ and remote sensing observations, *J. Geophys. Res.*, 108(D19), 8590, doi:10.1029/2002JD002659, 2003.
- Derimian, Y., Karnieli, A., Kaufman, Y. J., Andreae, M. O., Andreae, T. W., Dubovik, O., Maenhaut, W., Koren, I., and Holben, B. N.: Dust and pollution aerosols over the Negev desert, Israel: Properties, transport, and radiative effect, *J. Geophys. Res. D: Atmos.*, 111, 5, D05205, doi:10.1029/2005JD006549, 2006.
- di Sarra, A., Di Iorio, T., Cacciani, M., Fiocco, G., and Fua, D.: Saharan dust profiles measured by lidar at Lampedusa, *J. Geophys. Res.*, 106(D10), 10 335–10 347, 2001.
- Dubovik, O., Holben, B., Eck, T. F., Smirnov, A., Kaufman, Y. J., King, M. D., Tanre, D., and Slutsker, I.: Variability of absorption and optical properties of key aerosol types observed in worldwide locations, *J. Atmos. Sci.*, 59(3), 590–608, 2002a.
- Dubovik, O., Holben, B. N., Lapyonok, T., Sinyuk, A., Mishchenko, M. I., Yang, P., and Slutsker, I.: Non-spherical aerosol retrieval method employing light scattering by spheroids, *Geophys. Res. Lett.*, 29(10), doi:10.1029/2001GL014506, 2002b.
- Dubovik, O. and King, M. D.: A flexible inversion algorithm for retrieval of aerosol optical properties from Sun and sky radiance measurements, *J. Geophys. Res.*, 105(D16), 20 673–20 696, 2000.
- Dubovik, O., Sinyuk, A., Lapyonok, T., Holben, B. N., Mishchenko, M., Yang, P., Eck, T. F., Volten, H., Munoz, O., Veihermann, B., van der Zande, W. J., Leon, J. F., Sorokin, M., and Slutsker, I.: Application of spheroid models to account for aerosol particle nonsphericity in remote sensing of desert dust, *J. Geophys. Res.*, 111, D11208, doi:10.1029/2005JD006619, 2006.
- Dubovik, O., Smirnov, A., Holben, B. N., King, M. D., Kaufman, Y. J., Eck, T. F., and Slutsker, I.: Accuracy assessments of aerosol optical properties retrieved from Aerosol Robotic Network (AERONET) Sun and sky radiance measurements, *J. Geophys. Res.*, 105(D8), 9791–9806, 2000.
- Dulac, F. and Chazette, P.: Airborne study of a multi-layer aerosol structure in the eastern Mediterranean observed with the airborne polarized lidar ALEX during a STAAARTE campaign (7 June 1997), *Atmos. Chem. Phys.*, 31817–1831, 2003.

**Iron and black carbon
in aerosol light
absorption**Y. Derimian et al.

[Title Page](#)[Abstract](#)[Introduction](#)[Conclusions](#)[References](#)[Tables](#)[Figures](#)[◀](#)[▶](#)[◀](#)[▶](#)[Back](#)[Close](#)[Full Screen / Esc](#)[Printer-friendly Version](#)[Interactive Discussion](#)

**Iron and black carbon
in aerosol light
absorption**

Y. Derimian et al.

[Title Page](#)[Abstract](#)[Introduction](#)[Conclusions](#)[References](#)[Tables](#)[Figures](#)[◀](#)[▶](#)[◀](#)[▶](#)[Back](#)[Close](#)[Full Screen / Esc](#)[Printer-friendly Version](#)[Interactive Discussion](#)

- Falkowski, P. G.: Evolution of the nitrogen cycle and its influence on the biological sequestration of CO₂ in the ocean, *Nature*, 387, 6630, 272–275, 1997.
- Fan, S. M., Moxim, W. J., and Levy, H.: Aeolian input of bioavailable iron to the ocean, *Geophys. Res. Lett.*, 33, L07602, doi:10.1029/2005GL024852, 2006.
- 5 Fialho, P., Freitas, M. C., Barata, F., Vieira, B., Hansen, A. D. A., and Honrath, R. E.: The Aethalometer calibration and determination of iron concentration in dust aerosols, *J. Aerosol Sci.*, 37(11), 1497–1506, 2006.
- Fialho, P., Hansen, A. D. A., and Honrath, R. E.: Absorption coefficients by aerosols in remote areas: a new approach to decouple dust and black carbon absorption coefficients using seven-wavelength Aethalometer data, *J. Aerosol Sci.*, 36(2), 267–282, 2005.
- 10 Formenti, P., Andreae, M. O., Andreae, T. W., Galani, E., Vasaras, A., Zerefos, C., Amiridis, V., Orlovsky, L., Karnieli, A., Wendisch, M., Wex, H., Holben, B. N., Maenhaut, W., and Lelieveld, J.: Aerosol optical properties and large-scale transport of air masses: Observations at a coastal and a semiarid site in the eastern Mediterranean during summer 1998, *J. Geophys. Res.*, 106(D9), 9807–9826, 2001.
- 15 Formenti, P., Boucher, O., Reiner, T., Sprung, D., Andreae, M. O., Wendisch, M., Wex, H., Kindred, D., Tzortziou, M., Vasaras, A., and Zerefos, C.: STAAARTE-MED 1998 summer airborne measurements over the Aegean Sea - 2. Aerosol scattering and absorption, and radiative calculations, *J. Geophys. Res.*, 107(D21), 4451, doi:10.1029/2001JD001536, 2002a.
- 20 Formenti, P., Reiner, T., Sprung, D., Andreae, M. O., Wendisch, M., Wex, H., Kindred, D., Dewey, K., Kent, J., Tzortziou, M., Vasaras, A., and Zerefos, C.: STAAARTE-MED 1998 summer airborne measurements over the Aegean Sea – 1. Aerosol particles and trace gases, *J. Geophys. Res.*, 107(D21), 4221, doi:10.1029/2001JD001337, 2002b.
- Fung, I. Y., Meyn, S. K., Tegen, I., Doney, S. C., John, J. G., and Bishop, J. K. B.: Iron supply and demand in the upper ocean, *Global Biogeochem. Cycles*, 14(1), 281–295, 2000.
- 25 Ganor, E. and Foner, H. A.: The mineralogical and chemical properties and the behaviour of aeolian Saharan dust over Israel. *The Impact of Desert Dust Across the Mediterranean*. Guerzoni, S. and Chester, R. Printed in the Netherlands, Kluwer Academic Publishers, 163–172, 1996.
- 30 Gao, Y., Fan, S. M., and Sarmiento, J. L.: Aeolian iron input to the ocean through precipitation scavenging: A modeling perspective and its implication for natural iron fertilization in the ocean, *J. Geophys. Res.*, 108(D7), doi:10.1029/2002JD002420, 2003.
- Gao, Y., Kaufman, Y. J., Tanre, D., Kolber, D., and Falkowski, P. G.: Seasonal distributions of

- aeolian iron fluxes to the global ocean, *Geophys. Res. Lett.*, 28(1), 29–32, 2001.
- Gerasopoulos, E., Andreae, M. O., Zerefos, C. S., Andreae, T. W., Balis, D., Formenti, P., Merlet, P., Amiridis, V., and Papastefanou, C.: Climatological aspects of aerosol optical properties in Northern Greece, *Atmos. Chem. Phys.*, 3, 2025–2041, 2003,
5 <http://www.atmos-chem-phys.net/3/2025/2003/>.
- Guieu, C., Loye-Pilot, M. D., Ridame, C., and Thomas, C.: Chemical characterization of the Saharan dust end-member: Some biogeochemical implications for the western Mediterranean Sea, *J. Geophys. Res.*, 107(D15), doi:10.1029/2001JD000582, 2002.
- Hamonou, E., Chazette, P., Balis, D., Dulac, F., Schneider, X., Galani, E., Ancellet, G., and Pappayannis, A.: Characterization of the vertical structure of Saharan dust export to the Mediterranean basin, *J. Geophys. Res.*, 104(D18), 22 257–22 270, 1999.
- 10 Holben, B. N., Eck, T. F., Slutsker, I., Tanre, D., Buis, J. P., Setzer, A., Vermote, E., Reagan, J. A., Kaufman, Y. J., and Nakajima, T.: AERONET—A Federated Instrument Network and Data Archive for Aerosol Characterization, *Remote Sens. Environ.*, 66(1), 1–16, 1998.
- 15 Holben, B. N., Tanre, D., Smirnov, A., Eck, T. F., Slutsker, I., Abuhassan, N., Newcomb, W. W., Schafer, J. S., Chatenet, B., Lavenue, F., Kaufman, Y. J., Castle, J. V., Setzer, A., Markham, B., Clark, D., Frouin, R., Halthore, R., Karneli, A., O'Neill, N. T., Pietras, C., Pinker, R. T., Voss, K., and Zibordi, G.: An emerging ground-based aerosol climatology: Aerosol optical depth from AERONET, *J. Geophys. Res.*, 106(D11), 12 067–12 097, 2001.
- 20 Ichoku, C., Andreae, M. O., Andreae, T. W., Meixner, F. X., Schebeske, G., Formenti, P., Maenhaut, W., Cafmeyer, J., Ptasinski, J., Karnieli, A., and Orlovsky, L.: Interrelationships between aerosol characteristics and light scattering during late winter in an Eastern Mediterranean arid environment, *J. Geophys. Res.*, 104(D20), 24 371–24 393, 1999.
- Israelevich, P. L., Ganor, E., Levin, Z., and Joseph, J. H.: Annual variations of physical properties of desert dust over Israel, *J. Geophys. Res.*, 108(D13), 4381, doi:10.1029/2002JD003163, 2003.
- 25 Jacobson, M. Z.: Global direct radiative forcing due to multicomponent anthropogenic and natural aerosols, *J. Geophys. Res.*, 106(D2), 1551–1568, 2001.
- Jacobson, M. Z.: Climate response of fossil fuel and biofuel soot, accounting for soot's feedback to snow and sea ice albedo and emissivity, *J. Geophys. Res.*, 109, D21201, doi:10.1029/2004JD004945, 2004.
- 30 Jickells, T. D., An, Z. S., Andersen, K. K., Baker, A. R., Bergametti, G., Brooks, N., Cao, J. J., Boyd, P. W., Duce, R. A., Hunter, K. A., Kawahata, H., Kubilay, N., laRoche, J., Liss, P.

**Iron and black carbon
in aerosol light
absorption**Y. Derimian et al.

Title Page

Abstract

Introduction

Conclusions

References

Tables

Figures

◀

▶

◀

▶

Back

Close

Full Screen / Esc

Printer-friendly Version

Interactive Discussion

S., Mahowald, N., Prospero, J. M., Ridgwell, A. J., Tegen, I., and Torres, R.: Global iron connections between desert dust, ocean biogeochemistry, and climate, *Science*, 308, 5718, 67–71, 2005.

Johnson, K. S., Elrod, V. A., Fitzwater, S. E., Plant, J. N., Chavez, F. P., Tanner, S. J., Gordon, R. M., Westphal, D. L., Perry, K. D., Wu, J. F., and Karl, D. M.: Surface ocean-lower atmosphere interactions in the Northeast Pacific Ocean Gyre: Aerosols, iron, and the ecosystem response, *Global Biogeochem. Cycles*, 17(2), 2003.

Kaufman, Y. J., Boucher, O., Tanre, D., Chin, M., Remer, L. A., and Takemura, T.: Aerosol anthropogenic component estimated from satellite data, *Geophys. Res. Lett.*, 32, L17804, doi:10.1029/2005GL023125, 2005a.

Kaufman, Y. J., Koren, I., Remer, L. A., Tanre, D., Ginoux, P., and Fan, S.: Dust transport and deposition observed from the Terra-Moderate Resolution Imaging Spectroradiometer (MODIS) spacecraft over the Atlantic ocean, *J. Geophys. Res.*, 110, D10S12, doi:10.1029/2003JD004436, 2005b.

Kaufman, Y. J., Tanre, D., Dubovik, O., Karnieli, A., and Remer, L. A.: Absorption of sunlight by dust as inferred from satellite and ground-based remote sensing, *Geophys. Res. Lett.*, 28(8), 1479–1482, 2001.

Kirchstetter, T. W., Novakov, T., and Hobbs, P. V.: Evidence that the spectral dependence of light absorption by aerosols is affected by organic carbon, *J. Geophys. Res.*, 109, D21208, doi:10.1029/2004JD004999, 2004.

Koven, C. D. and Fung, I.: Inferring dust composition from wavelength-dependent absorption in Aerosol Robotic Network (AERONET) data, *J. Geophys. Res.*, 111, D14205, doi:10.1029/2005JD006678, 2006.

Kubilay, N., Cokacar, T., and Oguz, T.: Optical properties of mineral dust outbreaks over the northeastern Mediterranean, *J. Geophys. Res.*, 108(D21), 4666, doi:10.1029/2003JD003798, 2003.

Lafon, S., Rajot, J. L., Alfaro, S. C., and Gaudichet, A.: Quantification of iron oxides in desert aerosol, *Atmos. Environ.*, 38(8), 1211–1218, 2004.

Lafon, S., Sokolik, I. N., Rajot, J. L., Caquineau, S., and Gaudichet, A.: Characterization of iron oxides in mineral dust aerosols: Implications for light absorption, *J. Geophys. Res.*, 111, D21207, doi:10.1029/2005JD007016, 2006.

Maenhaut, W., Cafmeyer, J., Ptasiński, J., Andreae, M. O., Andreae, T. W., Elbert, W., Meixner, F. X., Karnieli, A., and Ichoku, C.: Chemical composition and light scattering of the atmo-

Iron and black carbon in aerosol light absorption

Y. Derimian et al.

Title Page

Abstract

Introduction

Conclusions

References

Tables

Figures

◀

▶

◀

▶

Back

Close

Full Screen / Esc

Printer-friendly Version

Interactive Discussion

spheric aerosol at a remote site in the Negev Desert, Israel, *J. Aerosol Sci.*, 28, Supplement 1, S73–S74, 1997.

Maenhaut, W., Salma, I., Cafmeyer, J., Annegarn, H. J., and Andreae, M. O.: Regional atmospheric aerosol composition and sources in the eastern Transvaal, South Africa, and impact of biomass burning, *J. Geophys. Res.*, 101(D19), 23 631–23 650, 1996a.

Maenhaut, W., Salomonovic, R., Cafmeyer, J., Ichoku, C., Karnieli, A., and Andreae, M. O.: Anthropogenic and natural radiatively active aerosol types at Sede Boker, Israel, *J. Aerosol Sci.*, 27, Supplement 1, S47–S48, 1996b.

Mahowald, N. M., Baker, A. R., Bergametti, G., Brooks, N., Duce, R. A., Jickells, T. D., Kubilay, N., Prospero, J. M., and Tegen, I.: Atmospheric global dust cycle and iron inputs to the ocean, *Global Biogeochem. Cycles*, 19, GB4025, 2005.

Martin, J. H. and Gordon, R. M.: Northeast Pacific Iron Distributions in Relation to Phytoplankton Productivity, *Deep-Sea Research Part a-Oceanographic Research Papers*, 35, 2, 177–196, 1988.

Mishchenko, M. I., Travis, L. D., Kahn, R. A., and West, R. A.: Modeling phase functions for dustlike tropospheric aerosols using a shape mixture of randomly oriented polydisperse spheroids, *J. Geophys. Res.*, 102(D14), 16 831–16 847, 1997.

Mongin, M., Nelson, D. M., Pondaven, P., and Treguer, P.: Simulation of upper-ocean biogeochemistry with a flexible-composition phytoplankton model: C, N and Si cycling and Fe limitation in the Southern Ocean, *Deep-Sea Research Part II-Topical Studies in Oceanography*, 53(5–7), 601–619, 2006.

Schkolnik, G., Chand, D., Hoffer, A., Andreae, M. O., Erlick, C., Swietlicki, E., and Rudich, Y.: Constraining the density and complex refractive index of elemental and organic carbon in biomass burning aerosol using optical and chemical measurements, *Atmos. Environ.*, 41(5), 1107–1118, 2007.

Schuster, G. L., Dubovik, O., Holben, B. N., and Clothiaux, E. E.: Inferring black carbon content and specific absorption from Aerosol Robotic Network (AERONET) aerosol retrievals, *J. Geophys. Res.*, 110, D10S17, doi:10.1029/2004JD004548, 2005.

Sinyuk, A., Dubovik, O., Holben, B., Eck, T. F., Breon, F. M., Martonchik, J., Kahn, R., Diner, D. J., Vermote, E. F., Roger, J. C., Lapyonok, T., and Slutsker, I.: Simultaneous retrieval of aerosol and surface properties from a combination of AERONET and satellite data, *Remote Sens. Environ.*, 107(1–2), 90–108, 2007.

Smirnov, A., Holben, B. N., Eck, T. F., Dubovik, O., and Slutsker, I.: Cloud-screening and

**Iron and black carbon
in aerosol light
absorption**

Y. Derimian et al.

Title Page

Abstract

Introduction

Conclusions

References

Tables

Figures

◀

▶

◀

▶

Back

Close

Full Screen / Esc

Printer-friendly Version

Interactive Discussion

quality control algorithms for the AERONET database, *Remote Sens. Environ.*, 73(3), 337–349, 2000.

Sokolik, I. N. and Toon, O. B.: Incorporation of mineralogical composition into models of the radiative properties of mineral aerosol from UV to IR wavelengths, *J. Geophys. Res.*, 104(D8), 9423–9444, 1999.

Stern, E., Gradus, Y., Meir, A., Krakover, S., and Tsoar, H.: *Atlas of the Negev*. Jerusalem, Keterpress Enterprises, 1986.

Tsidulko, M., Krichak, S. O., Alpert, P., Kakaliagou, O., Kallos, G., and Papadopoulos, A.: Numerical study of a very intensive eastern Mediterranean dust storm, 13–16 March 1998, *J. Geophys. Res.*, 107(D21), 4261, doi:10.1029/2001JD001168, 2002.

Watson, A. J., Bakker, D. C. E., Ridgwell, A. J., Boyd, P. W., and Law, C. S.: Effect of iron supply on Southern Ocean CO₂ uptake and implications for glacial atmospheric CO₂, *Nature*, 407, 6805, 730–733, 2000.

Wiggert, J. D., Murtugudde, R. G., and Christian, J. R.: Annual ecosystem variability in the tropical Indian Ocean: Results of a coupled bio-physical ocean general circulation model, *Deep-Sea Research Part II-Topical Studies in Oceanography*, 53(5–7), 644–676, 2006.

Zhang, X. Y., Gong, S. L., Shen, Z. X., Mei, F. M., Xi, X. X., Liu, L. C., Zhou, Z. J., Wang, D., Wang, Y. Q., and Cheng, Y.: Characterization of soil dust aerosol in China and its transport and distribution during 2001 ACE-Asia: 1. Network observations, *J. Geophys. Res.*, 108(D9), 4581, doi:10.1029/2002JD002632, 2003.

**Iron and black carbon
in aerosol light
absorption**

Y. Derimian et al.

Title Page

Abstract

Introduction

Conclusions

References

Tables

Figures

◀

▶

◀

▶

Back

Close

Full Screen / Esc

Printer-friendly Version

Interactive Discussion

Iron and black carbon in aerosol light absorption

Y. Derimian et al.

Table 1. Reported in literature and calculated percentage of Fe in total particulate mass (TPM) for several events and locations with dust-dominated conditions, and corresponding measured spectral single-scattering albedo for the study area and reported in literature. Calculated Fe is for an assumed BC_e percentage and accompanied by an error assessed for the worst scenario.

	Measured values in the study area and reported in literature		Calculated	Reported in literature
	$\omega_0(440\text{ nm})$	$\omega_0(1020\text{ nm})$	Fe, %TPM*	Fe, %TPM
Sede Boker, $\hat{a} < 0.6$, this work	0.91	0.96	2.86±1.00	2.9 (Ganor and Foner, 1996)
Solar Village, 13 June 2003 (Sinyuk et al., 2007)	0.90	0.94	2.70±0.98	-
Solar Village, 7 June 2003 (Sinyuk et al., 2007)	0.90	0.97	3.17±1.03	-
ASE-Asia, 12 April 2001 (Bergstrom et al., 2004)	0.85	0.95	3.64±1.08	3.9±0.5 to 4.0±0.9 (Zhang et al., 2003)
Senegal, 17 April 1987 (Kaufman et al., 2001)	0.86	0.99	4.11±1.14	4.45±0.49 (Guieu et al., 2002)

$Fe, \%TPM = \{[\omega_0(440) - \omega_0(1020)] - a2 \cdot BC_e\% - a3\} / a1$,
 where $a1 = -0.0635 \pm 0.0116$; $a2 = -0.002 \pm 0.0065$; $a3 = 0.1352 \pm 0.0429$ (\pm Std.Err.)

* Assumed $BC_e, \%TPM: 2.0 \pm 2.0\%$; Accuracy of $\omega_0(440) - \omega_0(1020): \pm 0.03$

Title Page

Abstract

Introduction

Conclusions

References

Tables

Figures

◀

▶

◀

▶

Back

Close

Full Screen / Esc

Printer-friendly Version

Interactive Discussion

**Iron and black carbon
in aerosol light
absorption**

Y. Derimian et al.

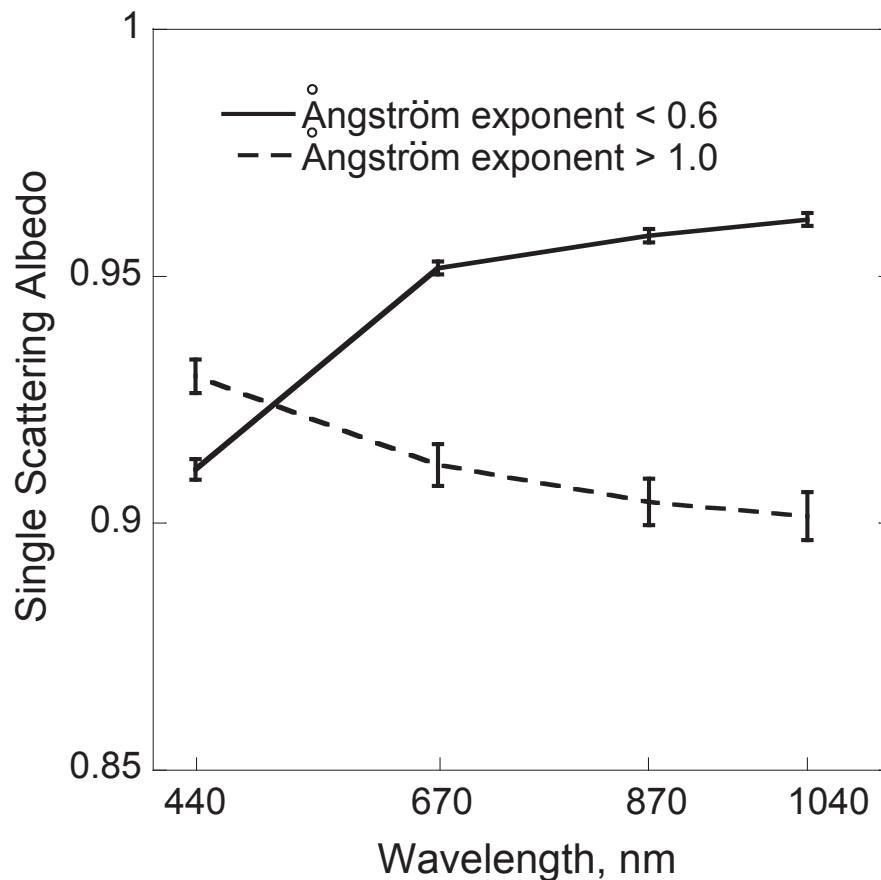


Fig. 1. Average spectral single-scattering albedo for periods with dominant contributions of coarse (Ångström exponent <0.6) and fine (Ångström exponent >1.0) aerosol for about eight years of measurements at the Sede Boker site.

[Title Page](#)[Abstract](#)[Introduction](#)[Conclusions](#)[References](#)[Tables](#)[Figures](#)[◀](#)[▶](#)[◀](#)[▶](#)[Back](#)[Close](#)[Full Screen / Esc](#)[Printer-friendly Version](#)[Interactive Discussion](#)

**Iron and black carbon
in aerosol light
absorption**

Y. Derimian et al.

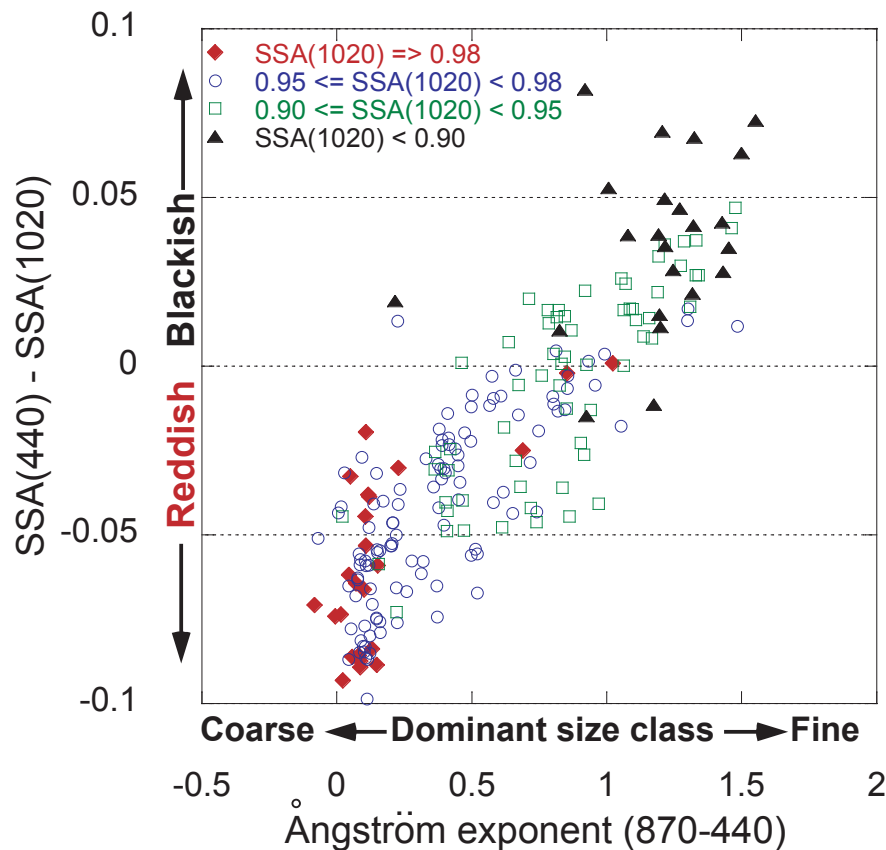


Fig. 2. Difference of $SSA(440\text{ nm}) - SSA(1020\text{ nm})$ versus Ångström exponent. All observations were conducted at the Sede Boker site from October 1995 to May 2006. Different ranges of $SSA(1020\text{ nm})$ values are presented by different symbols and indicate events from weak to strong absorption at 1020 nm.

[Title Page](#)[Abstract](#)[Introduction](#)[Conclusions](#)[References](#)[Tables](#)[Figures](#)[◀](#)[▶](#)[◀](#)[▶](#)[Back](#)[Close](#)[Full Screen / Esc](#)[Printer-friendly Version](#)[Interactive Discussion](#)

**Iron and black carbon
in aerosol light
absorption**

Y. Derimian et al.

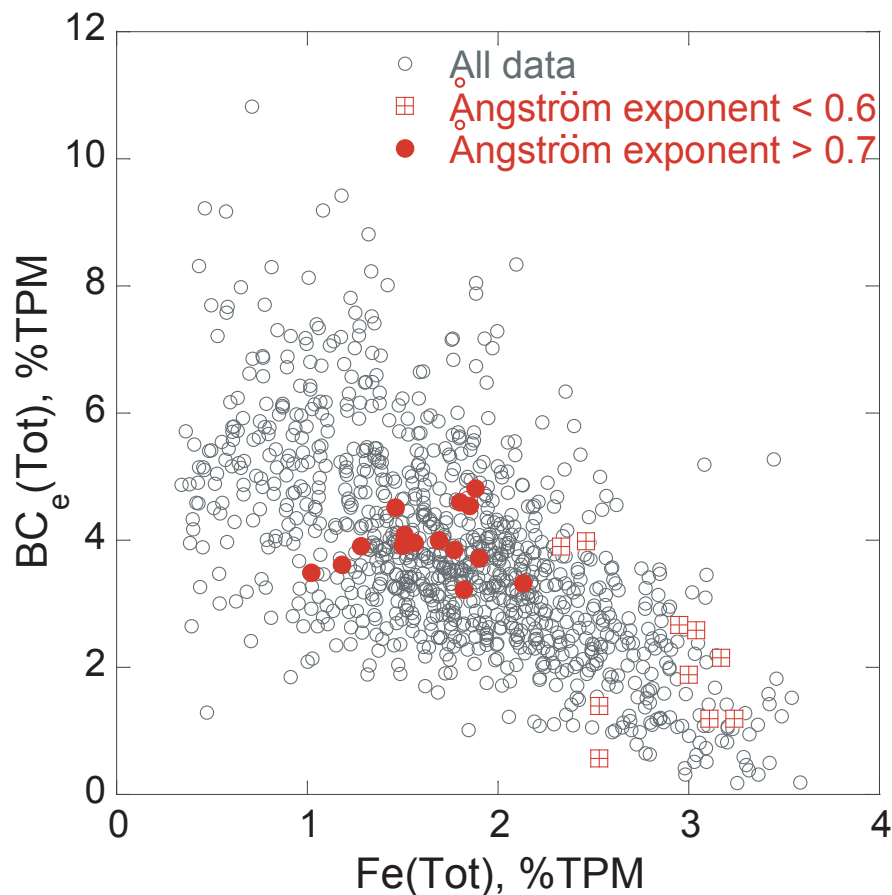


Fig. 3. BC_e percentage of the total particulate mass (BC_e, %TPM) versus Fe percentage of the total particulate mass (Fe, %TPM). Black open circles represent all available data, red solid circles (Ångström exponent < 0.6) and open squares (Ångström exponent > 0.7) represent a subset of data matched to optical column measurements.

**Iron and black carbon
in aerosol light
absorption**

Y. Derimian et al.

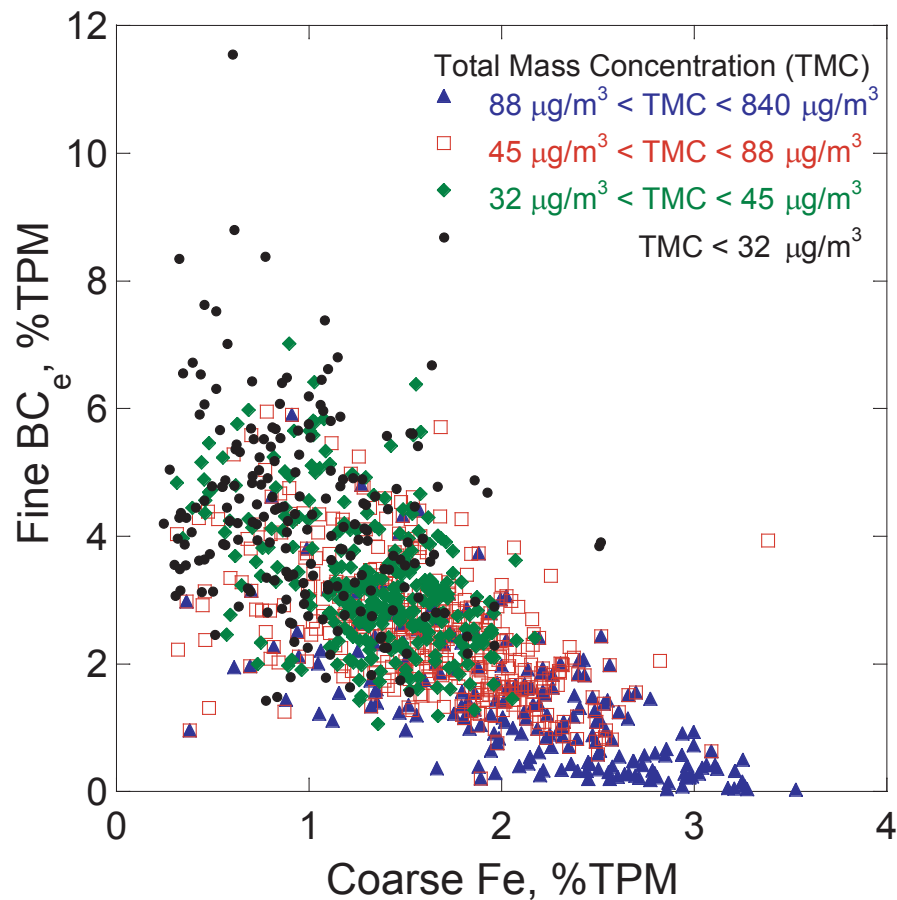


Fig. 4. BC_e, %TPM in the fine size fraction versus Fe, %TPM in the coarse size fraction. Different symbols indicate different ranges of total mass concentration.

[Title Page](#)[Abstract](#)[Introduction](#)[Conclusions](#)[References](#)[Tables](#)[Figures](#)[◀](#)[▶](#)[◀](#)[▶](#)[Back](#)[Close](#)[Full Screen / Esc](#)[Printer-friendly Version](#)[Interactive Discussion](#)

**Iron and black carbon
in aerosol light
absorption**Y. Derimian et al.

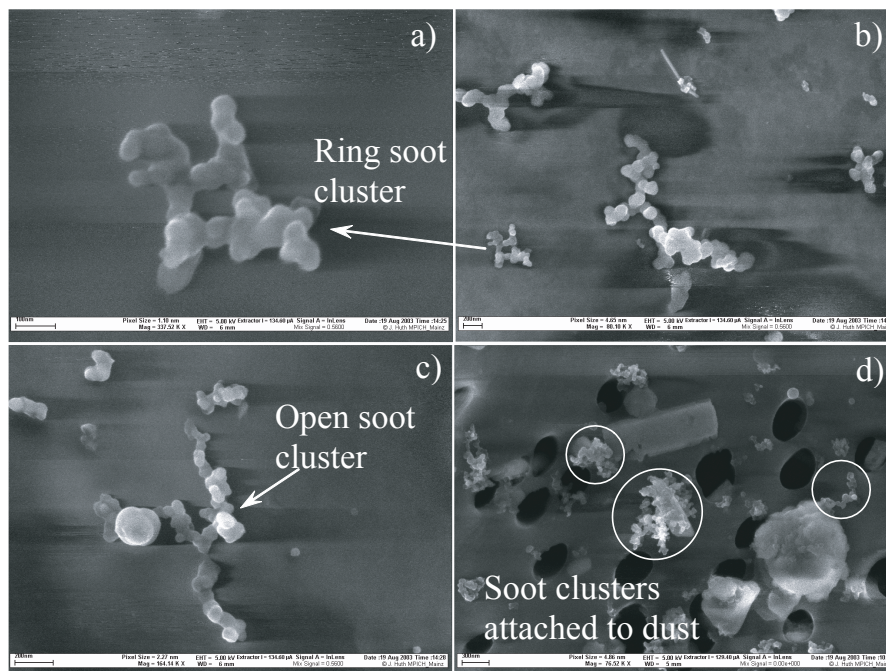


Fig. 5. Scanning electron microscope images of individual particles (a), (b), (c) demonstrate the presence of typical ring and open soot clusters that were found among dust particles on the coarse filter from the dust event on 2 April 2000, and (d) soot clusters attached to dust that were found on the fine filter from the dust event on 3 February 2001.

[Title Page](#)[Abstract](#)[Introduction](#)[Conclusions](#)[References](#)[Tables](#)[Figures](#)[◀](#)[▶](#)[◀](#)[▶](#)[Back](#)[Close](#)[Full Screen / Esc](#)[Printer-friendly Version](#)[Interactive Discussion](#)

**Iron and black carbon
in aerosol light
absorption**

Y. Derimian et al.

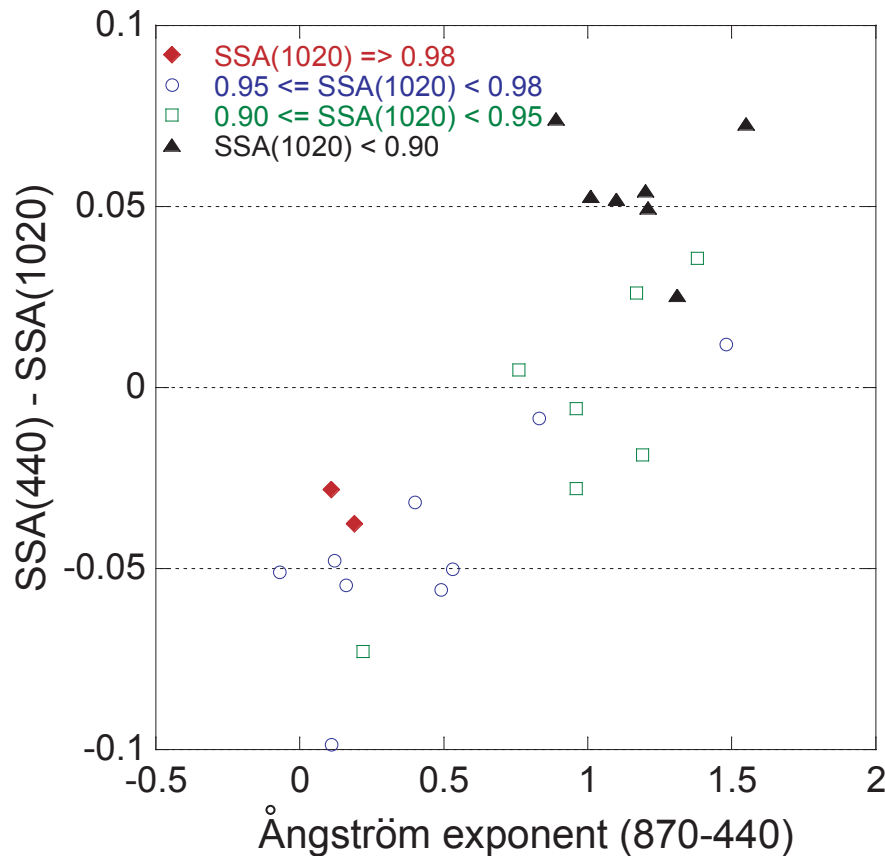


Fig. 6. Averaged values of the difference $\text{SSA}(440\text{ nm}) - \text{SSA}(1020\text{ nm})$ versus the Ångström exponent for 25 selected events measured during elevated loadings of dust and pollution aerosols. The presented data set was matched to the data set on aerosol chemistry.

[Title Page](#)[Abstract](#)[Introduction](#)[Conclusions](#)[References](#)[Tables](#)[Figures](#)[◀](#)[▶](#)[◀](#)[▶](#)[Back](#)[Close](#)[Full Screen / Esc](#)[Printer-friendly Version](#)[Interactive Discussion](#)

Iron and black carbon in aerosol light absorption

Y. Derimian et al.

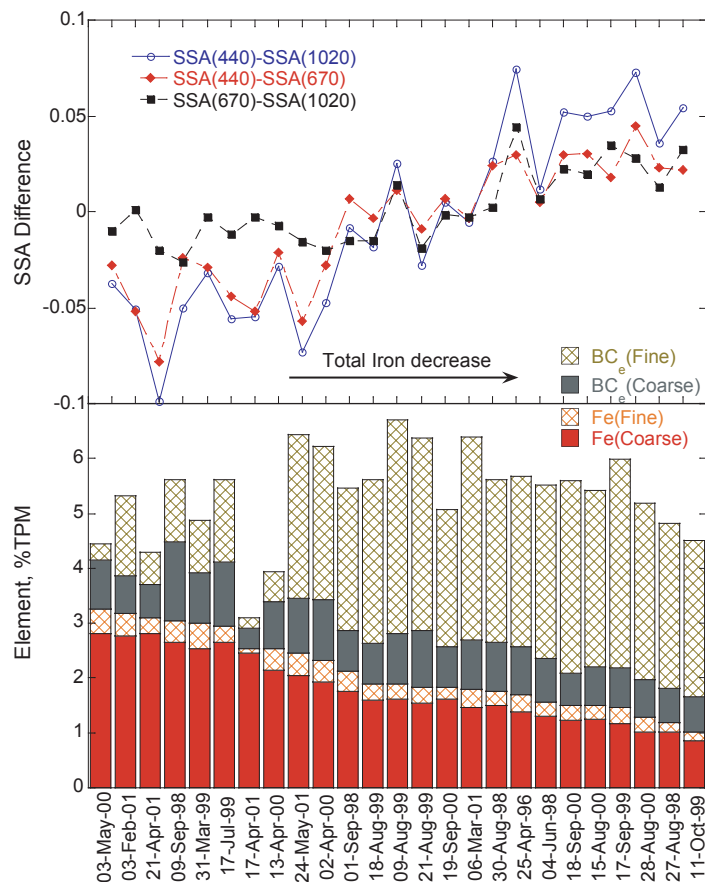


Fig. 7. BC_e and Fe percentage of the total particulate mass in the fine and coarse size fractions for 25 selected events and the corresponding differences of $SSA(440)-SSA(1020)$, $SSA(440)-SSA(670)$, and $SSA(670)-SSA(1020)$. The data are sorted by decreasing total iron concentration.

[Title Page](#)
[Abstract](#)
[Introduction](#)
[Conclusions](#)
[References](#)
[Tables](#)
[Figures](#)
[◀](#)
[▶](#)
[◀](#)
[▶](#)
[Back](#)
[Close](#)
[Full Screen / Esc](#)
[Printer-friendly Version](#)
[Interactive Discussion](#)